analytical chemistry

pubs.acs.org/ac Article

Direct Transverse Relaxation Time Biosensing Strategy for Detecting Foodborne Pathogens through Enzyme-Mediated Sol−Gel Transition of Hydrogels

Luyu Wei,[#] Zhilong Wang,[#] Caiwei Feng, Yunlei Xianyu,[*] and Yiping Chen[*]

Cite This: *Anal. Chem.* 2021, 93, 6613−6619 Read Online

ACCESS | Metrics & More | Article Recommendations | Supporting Information

ABSTRACT: In this work, we develop a direct transverse relaxation time (T_2) biosensing strategy and employ it for assaying foodborne pathogens relying on the alkaline phosphatase (ALP)-mediated sol−gel transition of hydrogels. ALP can catalyze the reaction to generate an acidic environment to transform the sol-state alginate solution to hydrogel, and this hydrogelation process can directly regulate the diffusion rate of water protons that results in a T_2 change of water molecules. By means of enzyme-modulated sol−gel transition and antigen−antibody interactions, this T_2 biosensor displays high sensitivity for detecting 50 CFU/mL *S. enteritidis* within 2 h. This biosensing strategy directly modulates the water molecules rather than magnetic probes in traditional methods, offering a straightforward, novel, and sensitive platform for pathogen detection.

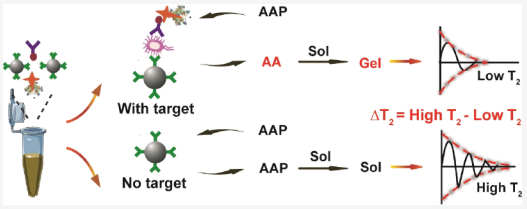

The issue of foodborne diseases caused by foodborne pathogen contamination has received considerable attention. According to the report from World Health Organization (WHO) in 2018, diarrheal diseases resulting from pathogen bacteria are the most common illnesses that cause 550 million illnesses and 33 million deaths each year. Therefore, it is critical to identify foodborne pathogens from contaminated food samples to prevent and control the outbreak of foodborne diseases. Traditional methods for pathogenic bacteria detection mainly rely on the serological validation of suspicious colonies[1] and the culture method known as the gold standard method owing to their high sensitivity and accuracy, but they are limited by the long detection time. For quantitative detection, polymerase chain reaction (PCR)-based nucleic acid assay[2] allows for accurate results, but sophisticated extraction and expensive equipment restrict its applications, particularly in resource-poor settings. Apart from nucleic acids, protein biomarkers of pathogenic bacteria have also been detected based on enzyme-linked immunosorbent assay (ELISA),[3] which is of low cost and is easy to use. However, traditional ELISA still suffers from limitations like relatively low sensitivity and time consumption. Therefore, it is still an urgent need to develop biosensing strategies with less detection time and enhanced sensitivity for foodborne pathogen detection.

Magnetic relaxation switching (MRS) biosensors[4] have attracted extensive attention for detecting foodborne pathogens because of their high sensitivity, low cost, and convenient operation. Compared to other biosensors such as electrochemical biosensors[5,6] and optical biosensors,[7,8] MRS biosensors based on a readout of transverse relaxation time (T_2) or longitudinal relaxation time (T_1) of hydrogen protons of water molecules are more attractive owing to the high signal-to-background ratio, rapidness, and facile operation. Currently, the principles of conventional MRS biosensors generally rely on dispersion/aggregation[9] or the quantity of magnetic nanoparticles (MNPs)[10] or the change of the valence state of paramagnetic ions such as Fe(II)/Fe(III),[11] Cu(II)/Cu(I),[12] and so forth.[13] All these sensing strategies are indirect ones that affect the magnetic probes first and then the relaxation behavior of the surrounding water molecules. These indirect sensing principles may suffer from limitations including the dispersion/aggregation instability of MNPs, the broad-size distribution of MNPs, and the relatively low sensitivity of paramagnetic ions. To address these issues, a more straightforward strategy could be developed that can directly and more effectively modulate the relaxation behavior of water molecules, thus circumventing the limitations of conventional MRS biosensors.

Acting as a dispersion medium, water molecules can be encapsulated in hydrogels through various cross-linking processes. Having features like three-dimensional (3D) network, pliability, and porous structure,[14] hydrogels are widely used in enzyme immobilization,[15] controlled drug delivery,[16] and tissue engineering.[17] Hydrogels such as alginate hydrogel, composite hydrogels,[18,19] and DNA hydrogels[20,21] have received increasing attention in biosensing because of

Received: September 19, 2020
Accepted: March 12, 2021
Published: April 22, 2021

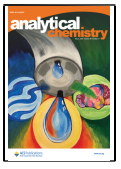

https://doi.org/10.1021/acs.analchem.0c03968
Anal. Chem. 2021, 93, 6613−6619

their sensitive response to pH or temperature, low toxicity, high availability, and low cost. The detection of pesticides,[22] heavy-metal ions,[23] and other biological molecules[24] has been demonstrated by the hydrogelation of alginate. For instance, organophosphorus pesticides can be detected based on the migration distance of alginate hydrogel on paper.[25] Previous work[26] has suggested that enzymes such as alkaline phosphatase (ALP) could trigger the hydrosol−hydrogel transition. This sol−gel transition can result in a change in the diffusion rate of water protons that leads to a change in the T_2 signal. This fact offers a promising biosensing platform for developing biosensors considering that ALP as a labeling enzyme has been widely used for immunoassays that can transform hydrosol to hydrogel, resulting in a T_2 signal readout.

In this study, we report a direct T_2 biosensing strategy by the ALP-mediated hydrogelation of alginate. Under the catalysis of ALP, the substrate 2-phospho-L-ascorbic acid trisodium salt (AAP) can be transformed to ascorbic acid (AA), and this H^+-containing molecule helps release Ca^{2+} from $CaCO_3$ that further reacts with the alginate solution to form alginate hydrogel[27,28] (Scheme 1A). By locking water molecules inside the "egg-box" network structure of alginate hydrogel,[29,30] it can significantly alter the transverse relaxation of water protons in aqueous solutions and result in a decrease in the T_2 value. The ALP-mediated hydrogelation of alginate can be used to modulate the T_2 signal, and based on this principle, we develop a T_2 biosensor via the ALP-mediated sol−gel transition of hydrogel that can be used for rapid and sensitive detection of foodborne pathogens. In this gelation-based T_2 biosensor, MNPs labeled with monoclonal capture antibody (Ab_1) and biotinylated-detection antibody (Ab_2) can identify the pathogen bacteria whose presence can result in the formation of MNPs-Ab_1-target-Ab_2-biotinylated-streptavidin-ALP complexes. ALP conjugated on the complex can then trigger the sol−gel transition of hydrogel that directly affects the relaxation behavior of water molecules, and the change of the T_2 value directly relates to the concentration of pathogenic bacteria (Scheme 1B).

Scheme 1. Schematic of Direct T_2 Biosensing Strategy through Enzyme-Mediated Sol−Gel Transition of Hydrogels for the Immunoassay of *S. enteritidis*[a]

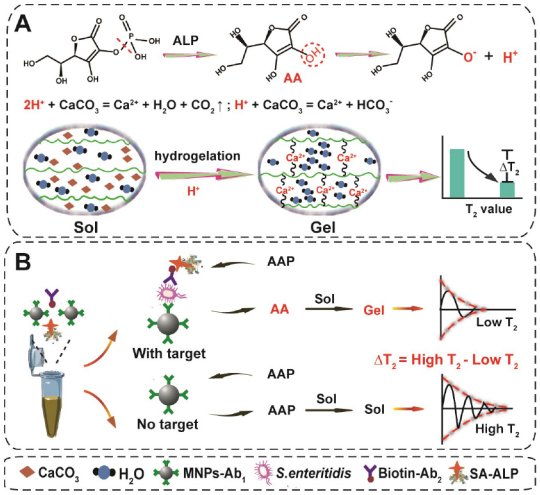

[a](A) ALP-catalyzed reaction to modulate the hydrogelation of sodium alginate with an "egg-box" network structure. (B) Schematic of gelation-based T_2 biosensor for detecting *S. enteritidis* whose presence helps form MNPss-Ab_1-antigen-Ab_2-biotin-streptavidin-ALP complex and produce AA that triggers the sol−gel transition of hydrogel to generate a significant change of the T_2 signal.

EXPERIMENTAL SECTION

Chemicals and Instrumentation. Carboxyl-modified MNPs (COOH-MNPs) (1000 nm, solid content: 10 mg/mL; 30 nm, solid content: 5 mg/mL) were purchased from Ocean NanoTech (USA). 2-Phospho-L-ascorbic acid trisodium salt (AAP), alkaline phosphatase (ALP), 1-ethyl-3-(3-dimethylaminopropyl)-carbodiimide hydrochloride (EDC), *N*-hydroxysulfosuccinimide sodium (sulfo-NHS), *N*, *N*-dimethylformamide (DMF), and sulfo-NHS-LC−LC−biotin were obtained from Sigma-Aldrich (USA). ALP-labeled streptavidin was purchased from Beyotime Biotechnology (Shanghai, China). Sodium alginate and calcium carbonate ($CaCO_3$) particles were obtained from Sinopharm Chemical Co., Ltd. (Shanghai, China). *S. enteritidis* (ATCC 14028), *Escherichia coli* (*E. coli*, ATCC 25922), *Listeria monocytogenes* (*L. monocytogenes*, ATCC 43257), *Staphylococcus aureus* (*S. aureus*, ATCC 29213), and *Vibrio parahaemolyticus* (*V. parahaemolyticus*, ATCC 17802) were obtained from the American Type Culture Collection (ATCC). Trypticase soy broth (TSB) and lysogeny broth (LB) were purchased from Qingdao Hope Bio-Technology Co., Ltd. (Qingdao, China). *Salmonella* core lipopolysaccharide monoclonal capture antibody (Ab_1, M374, 3.5 mg/mL) and detection antibody (Ab_2, M373, 2.1 mg/mL) were purchased from CalBioreagents Inc. (San Mateo, California, USA). Milk samples were purchased at local markets at Huazhong Agricultural University (Wuhan, China). Ultrapure water (resistivity ≥ 18 MΩ·cm) was used in the experiments. All other chemicals and reagents used were of analytical grade.

The SuperMag magnetic separator used in experiments was obtained from Ocean NanoTech (USA). A 0.5 T low-field nuclear magnetic resonance spectrometer (LF-NMR) used for T_2 measurements was purchased from Niumag Corp. (Shanghai, China). NMR imager and analyzer (NMI20-015 V-I) (Shanghai Niu-mag Corp.) was used to characterize the sol−gel transition of alginate hydrogel by magnetic resonance imaging (MRI). Rheological measurements were performed on a DHR-2 (TA Instruments) system, and 40 mm parallel plates were used during the experiment at the gap of 300 μm.

Preparation of MNPs-Ab_1 and Biotinylated-Ab_2 Conjugates. COOH-MNPs (100 μL) (1000 nm) was put into a 1.5 mL centrifuge tube and washed twice using MEST (10 mM MES, pH 6.0, containing 0.05% Tween 20). EDC (200 μL) (5 mg/mL) and 200 μL of NHS (5 mg/mL) were added to the tube for activation at room temperature for 30 min, and the solution was turned upside down with a rotary mixing instrument. After that, the excess EDC, NHS, and byproduct were removed via magnetic separation using a magnetic separator and were washed three times with MEST. Subsequently, 0.05 mg of Ab_1 was added to the activated MNP solution, and the mixture was gently stirred to react at 37 °C for 3 h and blocked with PBST (containing 10 mM PBS, pH 7.4, 0.05% Tween 20, and 1% BSA) for 0.5 h. The MNPs-Ab_1 conjugates were separated from free Ab_1 and washed four times with PBST. Finally, the resulting MNPs-Ab_1 conjugates were resuspended in 1 mL of PBST (containing 0.5% BSA) and stored at 4 °C for further use. The conjugates of MNP_{30}-

https://doi.org/10.1021/acs.analchem.0c03968
Anal. Chem. 2021, 93, 6613−6619

Ab_1 and MNP_{30}-Ab_2 were prepared based on the same method.

The preparation of biotinylated-Ab_2 conjugates was based on our previous work.[31] First, both sulfo-NHS-LC-biotin and Ab_2 were diluted to 1 mg/mL using DMF and PBS (pH = 7.4, 10 mM), respectively. Then, they were mixed at a molar ratio of 20:1 (NHS-LC−LC-biotin/Ab_2) and stirred for 4 h at room temperature for the biotinylation of Ab_2. After labeling, the solution was transferred into a clean dialysis bag (MW 10,000−14,000) for dialysis at 4 °C overnight to remove unreacted biotin. Finally, biotin-labeled Ab_2 was stored at 4 °C for further use.

Preparation of Alginate Sol Solution. Sodium alginate powder was dissolved in ultrapure water and stirred at 37 °C for 2 h to prepare 0.5% sodium alginate liquid solution, followed by the addition of premade $CaCO_3$ solution (30 mM) at a volume ratio of 1:1 (alginate sol/$CaCO_3$). Subsequently, the mixture was ultrasonicated for 30 min under 100 MPa pressure and was vortexed for 30 min to form a homogeneous suspension. The sodium alginate sol solution should be freshly prepared prior to use and should be free of particle aggregation and precipitation.

Bacteria Culture and Enumeration. All the bacterial strains mentioned above were stored at −80 °C with 15% glycerol and revived by growing on LB agar plates. *S. enteritidis* was grown in the TSB medium at 37 °C in a rotary shaker at 180 rpm overnight, and other bacterial strains were grown in the LB medium under the same conditions. For bacteria enumeration, 100 μL of bacterial solution was serially diluted with PBS, plated on LB agar plates, and incubated at 37 °C for 24 h. Then, we selected plates with colonies between 30 and 300 for counting and calculating the concentration, expressed as the number of colony-forming units per milliliter (CFU/mL).

Procedure for *S. enteritidis* Detection by Enzyme-Mediated T_2 Biosensors. First, 400 μL of *S. enteritidis* of gradient dilutions (10^1−10^7) were separately incubated with 100 μL of MNPs-Ab_1 for 30 min at 37 °C in 1.5 mL sterile centrifuge tube. The sterile PBS was used as a negative control. After that, MNPs-Ab_1 with the captured bacteria was collected by a magnetic scaffold and washed three times with PBST (pH 7.4, 0.05% Tween 20). The MNPs-Ab_1-*S. enteritidis* complexes were then resuspended using 400 μL of PBS and added into 100 μL of biotinylated-Ab_2 to gently react at 37 °C for 30 min. After magnetic separation and washing three times with PBST, 100 μL of SA-ALP and 300 μL of PBS were added into each tube to gently react at 37 °C for 30 min. After magnetic separation and washing four times with PBST, the MNPs-Ab_1-*S. enteritidis*-Ab_2-ALP complexes were mixed with 100 μL of AAP and 200 μL of ultrapure water and washed twice with 200 μL of ultrapure water after reaction at 37 °C for 30 min. Finally, the collected AA by magnetic separation was added to the alginate sol solution to react for 5 min, which could cause the hydrogelation of alginate. The transverse relaxation time (T_2) of the solution was measured by low-field nuclear magnetic resonance (LF-NMR). The Carr−Purcell−Meiboom−Gill (CPMG) pulse sequence was employed for T_2 measurements with the following parameters: NMR frequency, 19.894 MHz; 90° pulse width, 13 μs; 180° pulse width, 26 μs; TW = 4000 ms; NECH = 4000 ms; SW = 100 KHz; TE = 1.0 ms; NS = 2; We used a simultaneous iterative reconstruction technique (SIRT) based on a whole iterative correction multi-index inversion algorithm to obtain the T_2 signal from the CPMG decay curve on the instrument. Each data point was performed three times to obtain the average and the standard deviation.

Procedure for *S. enteritidis* Detection by Magnetic Separation−MRS Approach and MNP-Mediated MRS Approach. In the MS−MRS approach, 100 μL of MNP_{1000}-Ab_1 solution, 100 μL of MNP_{30}-Ab_2 solution, and 800 μL of different concentrations of *S. enterica* (10^7, 10^6, 10^5, 10^4, 10^3, 5×10^2, 2×10^2, 10^2, and 0 CFU/mL) were transferred to individual 1.5 mL centrifuge tubes. Each mixture was gently shaken for 30 min. All the tubes were then placed on a magnetic separator for 1 min, and 200 μL of supernatant of each tube was transferred into a 7.5 mm NMR tube for T_2 measurements. The CPMG pulse sequence was employed for T_2 measurements with the following parameters: NMR frequency, 19.894 MHz; 90° pulse width, 13 μs; 180° pulse width, 26 μs; TW = 1000 ms; NECH = 1000 ms; SW = 100 KHz; TE = 1.0 ms; NS = 2. Each data point was performed three times to obtain the average and the standard deviation.

In the MNP-mediated MRS approach, 50 μL of MNP_{30}-Ab_1 solution and 200 μL of *S. enteritidis* of different concentrations (0, 800, 900, 10^3, 10^4, 10^5, 10^6, and 10^7 CFU/mL) were transferred to 1.5 mL centrifuge tubes. Each mixture solution was gently shaken for 30 min at 37 °C. Then, 50 μL of MNP_{30}-Ab_2 solution was added into each tube to gently react at 37 °C for 30 min. Finally, T_2 of the mixture solution was detected by LF-NMR. The detection parameters were the same as above.

Preparation of the Spiked Milk Samples. Milk was selected as the food matrix to prepare samples of artificially contaminated *S. enteritidis*. First, the *S. enteritidis* solution was serially diluted into 10^5 to 10^8 CFU/mL with PBS. Five milk samples of 5 mL were prepared and placed in a 10 mL sterile centrifuge tube. After that, 100 μL of *S. enteritidis* was added to prepare the spiked milk samples with the bacterial concentrations from 2×10^3 to 2×10^6 CFU/mL for the immunomagnetic separation and MRS sensing. The recovery rate by hydrogel-mediated T_2 sensing is calculated using the following formula: $P\% = C_1/C_0 \times 100\%$, where C_1 represents the number of bacteria detected with this T_2 biosensor, and C_0 is the initial number of bacteria added into the milk sample.

RESULTS AND DISCUSSION

Principle of Alginate Hydrogelation for T_2 Sensing. Calcium alginate hydrogel exhibits good stability because of the strong interactions between Ca^{2+} and alginate. Water molecules can form hydrogen bonds after hydrogelation, and the hydrogel can maintain its gel state. Numerous water molecules would be locked in the hydrogel that can be directly employed to modulate the T_2 signal. We first used different concentrations of $CaCl_2$ to directly react with sodium alginate for the T_2 measurement. As shown in Figure 1A, magnetic resonance imaging (MRI) indicated the density of the hydrogel networks and the relaxation behaviors of water protons locked in hydrogels. The T_2-weighed MRI images suggest that a higher concentration of $CaCl_2$ would result in a higher density of the hydrogel and therefore a weaker signal of the image because of the shortened T_2 value. This is because the amount of Ca^{2+} ions can greatly influence the formation of calcium alginate hydrogel. We further quantified the shortened T_2 value showing that an optimal concentration of 25 mM Ca^{2+} was beneficial for the hydrogel formation (Figure 1B). The optimized concentration of sodium alginate and reaction time were 0.2% and 15 min, respectively, and the formed

https://doi.org/10.1021/acs.analchem.0c03968
Anal. Chem. 2021, 93, 6613−6619

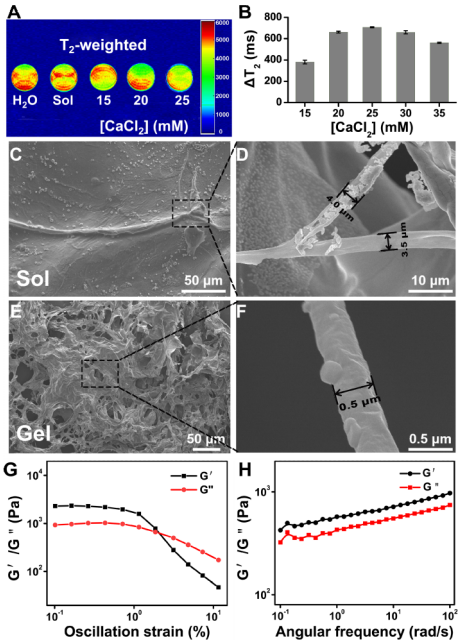

Figure 1. MRI, SEM, and rheological characterizations of the sol−gel transition of alginate hydrogel. (A) MRI images of H_2O, alginate sol solution, and alginate hydrogel induced by $CaCl_2$ with concentrations of 15, 20, and 25 mM. (B) Optimization of the $CaCl_2$ concentration for the T_2 signal change. SEM images of alginate (C, D) before hydrogelation and (E, F) after hydrogelation. (G) Oscillation strain sweep of hydrogel in the range of 0.1−10%. (H) Angular frequency sweep of the hydrogel. The rheological measurement was performed at 25 °C, with the frequency of 1 Hz and strain of 1% for strain sweep and frequency sweep separately. Error bars represent the standard deviation of three replicates (n = 3).

hydrogel could be visualized by the naked eye (Figure S1). Compared with the sol solution, the T_2 signal changed significantly after the formation of calcium alginate hydrogel, mainly because of the changes in the migration and movement of water molecules.[26] In addition, the gel solution was characterized by scanning electron microscopy (SEM). Prior to hydrogelation, the sodium alginate-lyophilized solution appeared as a rough film instead of micropores, and the diameter of the rodlike fiber was between 3.5 and 4.0 μm (Figure 1C,D). In contrast, the hydrogelation resulted in an "egg-box" structure, and the diameter of the rod-shaped fibers was 0.5 μm, which is at least 7 times lower than that before hydrogelation (Figure 1E,F). This might be due to the ion exchange between Ca^{2+} and the alginic inner wall, resulting in a more compact structure.[32] These results show that the calcium alginate hydrogel could lock water molecules inside and thus change the relaxation time of the solution during the sol−gel transition.

To evaluate the stability of the T_2 signal over time, the ability of the hydrogel to retain water molecules thus affecting the relaxation behavior was measured. We directly used an optimized concentration of $CaCl_2$ (25 mM) to react with the carboxylate of sodium alginate and recorded the change of weight after incubation for different times at 37 °C. Thereafter, water retention (WR) was calculated using the formula: WR = $[1-(W_0-W_n)/W_0] \times 100\%$, where W_0 represents the original weight of the hydrogel, and W_n represents the weight of the hydrogel after incubation. Results showed that the formed hydrogel was able to retain more than 97% water in an hour (Figure S2). In addition, rheological measurements were performed to evaluate the viscoelasticity of the hydrogel. Viscoelasticity, as one of the most important features of hydrogel, is commonly used to illustrate its mechanical properties. Elasticity can reflect the solid-like behavior while viscosity can reflect the liquid-like behavior. The sol−gel transition of hydrogel in this assay can be evaluated by the viscoelasticity of the hydrogel, which can reveal whether the water molecules are locked in the hydrogel. In addition, it can also reveal the robustness of the hydrogel that decides the stability of T_2. As shown in Figure 1G, the storage modulus (G') and loss modulus (G'') of the solution are almost constant below 1% strain, then decline dramatically with the increase of oscillation strain. It is worth noting that $G' > G''$ below 1% strain, indicating that the solution behaves as hydrogels. We then set the strain within the linear viscoelastic region for a dynamic frequency sweep. G' and G'' both slightly increase when the angular frequency is from 0.1 to 100 rad/s, while the values of G' dominate over those of G'' all the time (Figure 1H), showing excellent stability and mechanical properties of hydrogel. It suggests that the prepared hydrogel can firmly lock water inside, making a more reliable measured T_2 value.

Sol−Gel Transition Triggered by AA and ALP. The sol−gel transition can be triggered by small molecules and enzymes such as AA and ALP. AA contains H^+ and can transform insoluble $CaCO_3$ to Ca^{2+}, which can trigger the hydrogelation of calcium alginate. Based on this principle, this sol−gel transition can be utilized to develop biosensors for detecting AA and ALP. To investigate the sensitivity of this T_2 biosensor to AA (Figure 2A), different concentrations of AA (500, 200, 100, 50, 10, 5, 1, 0.1, 0.01, and 0 μM) were incubated with alginate sol solution and transferred to a LF-

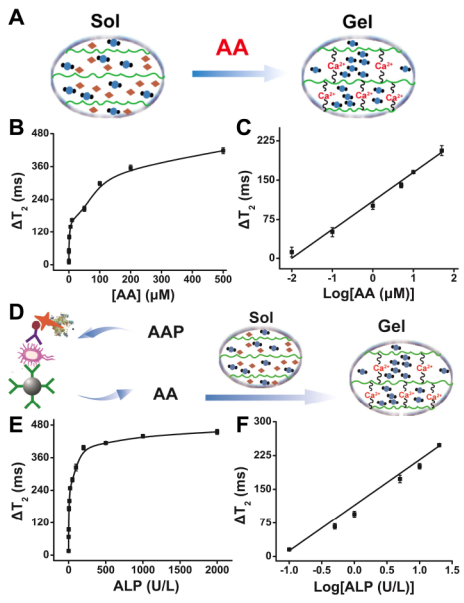

Figure 2. Biosensors based on sol−gel transition triggered by AA and ALP. (A) Schematic of the sol−gel transformation-based T_2 sensor for AA detection, (B) standard curve, (C) linear range for the detection of AA. The concentration of AA is from 0 to 500 μM.(D) Schematic of the sol−gel transformation-based T_2 for ALP detection, (E) standard curve, (F) linear range for the detection of ALP. The activity of ALP is from 0 to 1000 U/L. Error bars represent the standard deviation of three replicates (n = 3).

https://doi.org/10.1021/acs.analchem.0c03968
Anal. Chem. 2021, 93, 6613−6619

NMR tube for the determination of the T_2 value. As shown in Figure 2B, ΔT_2 increases when the concentration of AA increases from 0.01 to 500 μM, and the linear range of hydrogel-mediated AA detection is from 0.01 to 50 μM (Y = 54.86X + 110.0, X = log [AA (μM)], R^2 = 0.99) (Figure 2C). The limit of detection (LOD) of AA is 0.026 μM, where LOD = 3S/M, S is the value of the standard deviation of blank samples, and M is the slope of the standard curve within a low concentration range.

This sol−gel transition can be also employed to develop an ALP biosensor considering that ALP can catalyze the reaction to generate AA (Figure 2D). Because AA can be obtained through the hydrolysis of substrate (AAP), we first investigated the changes of the T_2 value under different concentrations of AAP and found that 10 mM AAP is suitable (Figure S3). Based on the optimized concentrations, we developed an ALP assay by studying the relationship between the T_2 value and different amounts of ALP (1000, 500, 100, 10, 1, 0.5, 0.1, 0.01 U/L). As shown in Figure 2E,F, there is a significant correlation between the increase of the ΔT_2 value and the activity of ALP, and it has a good linear correlation with R^2 = 0.996 (Y = 101.44X + 114.19, X = log [ALP (U/L)]).

Gelation-Based T_2 Biosensor through Sol−Gel Transition. Because ALP can act as a labeling enzyme for immunoassays, this sol−gel transition-based T_2 biosensor can be employed for immunoassays that have a T_2 signal readout. To achieve this, we first optimize the conditions of several key parameters for the immunoassays. Their effects on the T_2 signal were investigated by a single factor method to ensure good sensitivity. In this T_2 biosensor, the concentration of biotinylated-Ab_2 conjugates involved in the sandwich immunostructure and the amounts of streptavidin labeled-ALP are of great importance. Because streptavidin theoretically has four binding sites to interact with biotin, we make the molar ratio of streptavidin and biotin as 1: 4 and study the sensitivity. It shows a good concentration-dependent relationship when the dilution ratio is 1: 1200 but not when it is 1: 1000 or 1: 1500 (Figure S4A). The excess SA-ALP can nonspecifically bind to the surface of the immunocomplex, leading to insignificant changes of the T_2 signal. Meanwhile, less SA-ALP can generate AA insufficiently that decreases the sensitivity. Similarly, the dilution ratio of biotin-Ab_2 (Figure S4B) and MNPs-Ab_1 are also optimized to ensure the sensitivity (Figure S4C).

Gelation-Based T_2 Biosensor for *S. enteritidis* Detection. Under optimized conditions, the sensitivity of *S. enteritidis* detection was evaluated (Figure 3A). As shown in Figure 3B, the ΔT_2 value has a significant increase when the concentration of *S. enteritidis* ranges from 50 to 2 × 10^7 CFU/mL. The increment of T_2 is up to 250 ms in a concentration of 10^7 CFU/mL for *S. enteritidis*, which is approximately fifth of the initial magnitude. The standard curve for *S. enteritidis* in PBS was linear within the concentration ranges from 2 × 10^2 to 2 × 10^6 CFU/mL (Figure 3C), which is well fitted using a linear equation Y = 44.67X − 36.48 (X = log [*S. enteritidis* (CFU/mL)]), with R^2 = 0.997. The LOD was 43 CFU/mL, with the same calculated formula of AA. As a comparison, the sensitivity and linear range of the MS−MRS-based sensor and the MNP-mediated MRS approach for detecting *S. enteritidis* were studied. In the MS-MRS approach, after the antigen−antibody reaction, we employed a magnetic field of 0.01 T to separate the magnetic beads of large size (1000 nm in diameter) from those of small size (30 nm in diameter) and used T_2 of the water molecules around the 30 nm magnetic

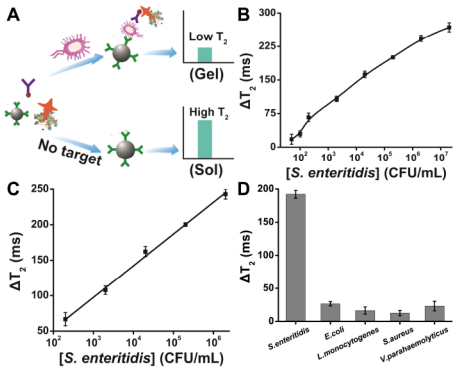

Figure 3. Sensitivity and specificity of the sol−gel transition-based T_2 biosensor for detecting *S. enteritidis*. (A) Scheme of enzyme-mediated sol−gel transition-based T_2 biosensor for *S. enteritidis* detection. (B) Standard curve for detecting *S. enteritidis*, and different concentrations of *S. enteritidis* ranging from 50 to 2 × 10^7 CFU/mL. (C) Linear range and (D) specificity for detecting *S. enteritidis*. The concentrations of all bacteria are 10^5 CFU/mL. Error bars represent the standard deviation of three replicates (n = 3).

beads (MB_{30}) as the signal readout of the immunoassay (Figure S5A). The linear range of MS−MRS for detecting *S. enteritidis* was from 10^4 to 10^7 CFU/mL, and the linear equation was Y = 38.91X−112.95 (X = log [*S. enteritidis* (CFU/mL)]) with R^2 = 0.990. The LOD was 100 CFU/mL. The increment of T_2 is merely approximately 150 ms even in a high concentration of 10^7 CFU/mL for *S. enteritidis*, and the signal change (ΔT_2) is not remarkable which is just one in twenty of the initial magnitude (Figures S5B and S5C). In the MNP-mediated MRS approach, the antigen−antibody interaction leads to the aggregation of MNPs and indirectly modulates the relaxation behavior of water molecules (Figure S6A). The linear range of MNP-mediated MRS for detecting *S. enteritidis* was from 10^3 to 10^6 CFU/mL, and the linear equation was Y = 10.3X − 14.9 (X = log [*S. enteritidis* (CFU/mL)]) with R^2 = 0.998; the LOD was 800 CFU/mL. The signal change of T_2 is less than 50 ms even in a high concentration of 10^7 CFU/mL for *S. enteritidis*, which is just one in thirty of the initial magnitude (Figures S6B and S6C). These results show that the sol−gel transition-based T_2 sensor exhibits better performance than the MS−MRS approach and MNP-mediated MRS approach, suggesting that the sol−gel transition is effective in enhancing the sensitivity. Although the sol−gel transition-based method can complete the whole detection within 2 h, it is still slightly inferior to the abovementioned two methods because of the introduction of the biotin−streptavidin system and the enzymatic reaction. Future study will focus on decreasing the detection time while maintaining the high sensitivity of this proposed approach. More importantly, this sol−gel transition-based T_2 sensor exhibits better performance than other reported methods (Table S1), primarily ascribed to the direct modulation of the relaxation behavior of water molecules, the high efficiency of immunomagnetic separation, and the biotin−streptavidin signal amplification.

The specificity was evaluated by performing immunoassay using four other common pathogenic bacteria, including *S. aureus*, *E. coli*, *V. parahaemolyticus*, and *L. monocytogenes*. As shown in Figure 3D, at the same concentration, only *S. enteritidis* can induce a significant change of the ΔT_2 value, while other bacteria have a negligible effect. The results prove

https://doi.org/10.1021/acs.analchem.0c03968
Anal. Chem. 2021, 93, 6613−6619

that the method has high specificity for *S. enteritidis*, attributing to the highly selective binding of monoclonal antibodies to the target bacteria.

To evaluate the accuracy of the gelation-based T_2 biosensor in real samples, we tested a series of concentrations of spiked milk samples from 2×10^3 to 2×10^6 CFU/mL, showing that the average recoveries ranged from 83.5 to 121% with the relative standard derivations (RSDs) from 3.07 to 5.08% (Table 1). The low RSDs and high recovery in the spiked experiments indicated that this approach has great potential for detecting *S. enteritidis* in real samples.

Table 1. Recovery Rate of the Sol−Gel Transition-Based T_2 Sensor for Detecting *S. enteritidis* in Spiked Milk Samples

spiked (CFU/mL)	found (CFU/mL)	recovery (%)	RSD (%)
2×10^3	1.67×10^3	83.5	4.58
2×10^4	1.82×10^4	91	5.08
2×10^5	1.91×10^5	95.5	3.07
2×10^6	2.42×10^6	121	4.96

Real Sample Analysis. To evaluate the real-world applicability of the designed method, we employed it to detect *S. enteritidis* in 20 milk samples and used MS−MRS approach for comparison. All these samples were predetermined using the culture method. Results showed that all the positive samples (samples 4, 9, 12, and 15) were detected positive using the hydrogel-mediated approach, which shows good consistency with the gold standard culture method. In contrast, only sample 4 and sample 15 were detected positive by MS−MRS because of its insufficient sensitivity. All the other sixteen negative samples were detected negative using both methods (Figure 4). The P value is calculated to be 0.004 by a paired-samples t-test ($P < 0.01$), suggesting that the observed ΔT_2 between this method and the MS−MRS approach/background has an extremely significant difference. These results indicate that sol−gel transition-based T_2 biosensor exhibits higher accuracy than the MS-MRS approach for *S. enteritidis* detection.

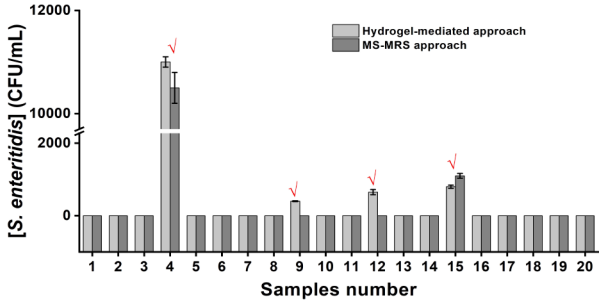

Figure 4. Comparison of the hydrogel-mediated approach and the MS−MRS approach for *S. enteritidis* detection in real milk samples. "√" represents positive samples. Error bars represent the standard deviation of three replicates ($n = 3$).

The gelation-based T_2 biosensor not only retains the advantages of conventional biosensors such as good sensitivity and rapid response but also has better stability over conventional one that enables pathogen detection with both high sensitivity and stability. Despite these merits, this gelation-based assay also has several issues that need to be addressed. Currently, this approach can be merely applied in limited samples with simple food matrix. It cannot realize the simultaneous detection of multiple targets. Therefore, considerable efforts should be made toward multiplex detection by simplifying the detection procedure. In addition, the development of the pretreatment method is also beneficial for its broader applications in complicated food matrix.

CONCLUSIONS

In summary, we report a T_2 biosensing strategy by directly modulating the relaxation behavior of water molecules using ALP-mediated sol−gel transition of hydrogels. Taking advantages of the immunomagnetic separation and enzyme-controlled hydrogelation, we develop a gelation-based T_2 biosensor for highly sensitive and specific detection of *S. enteritidis*. Compared with MS−MRS and MNP-mediated MRS, the enzyme-mediated sol−gel transition-based T_2 biosensor can directly alter the relaxation behavior of water molecules, more efficiently affecting the T_2 value. In future work, we will focus on straightforward strategies for more efficiently modulating the T_2 value of water molecules that can greatly improve the sensitivity and shorten the detection time.

ASSOCIATED CONTENT

Supporting Information

The Supporting Information is available free of charge at https://pubs.acs.org/doi/10.1021/acs.analchem.0c03968.

Optimization of the concentration of sodium alginate and the reaction time and photograph of alginate before and after hydrogelation, water retention of the hydrogel as time changes, changes of the T_2 value under different concentrations of AAP, condition optimization of T_2-based immunoassay through sol−gel transition, MS−MRS approach for detecting *S. enteritidis*, MNP-mediated MRS approach for detecting *S. enteritidis*, and comparison of the developed method with the reported methods for the detection of *Salmonella* (PDF)

AUTHOR INFORMATION

Corresponding Authors

Yunlei Xianyu − *College of Biosystems Engineering and Food Science, Zhejiang University, Hangzhou 310058, Zhejiang, China; Ningbo Research Institute, Zhejiang University, Ningbo 315100, Zhejiang, China*; Email: xianyu19@zju.edu.cn

Yiping Chen − *College of Food Science and Technology, Huazhong Agricultural University, Wuhan 430070, Hubei, China; Key Laboratory of Environment Correlative Dietology, Huazhong Agricultural University, Ministry of Education, Wuhan 430070, Hubei, China*; orcid.org/0000-0001-9309-2730; Email: chenyiping@mail.hzau.edu.cn

Authors

Luyu Wei − *College of Food Science and Technology, Huazhong Agricultural University, Wuhan 430070, Hubei, China; Key Laboratory of Environment Correlative Dietology, Huazhong Agricultural University, Ministry of Education, Wuhan 430070, Hubei, China*

Zhilong Wang − *College of Food Science and Technology, Huazhong Agricultural University, Wuhan 430070, Hubei, China; Key Laboratory of Environment Correlative*

https://doi.org/10.1021/acs.analchem.0c03968
Anal. Chem. 2021, 93, 6613−6619

Dietology, Huazhong Agricultural University, Ministry of Education, Wuhan 430070, Hubei, China

Caiwei Feng − *Beijing Kwinbon Biotechnology Co., Ltd., Beijing 100190, China*

Complete contact information is available at: https://pubs.acs.org/10.1021/acs.analchem.0c03968

Author Contributions

[#]L.W. and Z.W. contributed equally to this work.

Notes

The authors declare no competing financial interest.

■ ACKNOWLEDGMENTS

We thank the National Key R&D Program of China (2019YFC1605502, 2020YFA0909100), Wuhan Applied Foundational Frontier Project (2019020701011426), Beijing Nova Program (Z181100006218017), and the "Hundred Talents Program" from Zhejiang University for financial support.

■ REFERENCES

(1) Sheikhzadeh, E.; Chamsaz, M.; Turner, A. P. F.; Jager, E. W. H.; Beni, V. *Biosens. Bioelectron.* **2016**, *80*, 194−200.
(2) Tao, J.; Liu, W. W.; Ding, W.; Han, R.; Shen, Q.; Xia, Y.; Zhang, Y. H.; Sun, W. P. *J. Food Sci.* **2020**, *85*, 744−754.
(3) He, Y. X.; Ren, Y. R.; Guo, B.; Yang, Y. F.; Ji, Y. W.; Zhang, D. H.; Wang, J. L.; Wang, Y. R.; Wang, H. *Food Chem.* **2020**, *310*, No. 125942.
(4) Zhang, Y.; Yang, H.; Zhou, Z. G.; Huang, K.; Yang, S. P.; Han, G. *Bioconjugate Chem.* **2017**, *28*, 869−879.
(5) Capobianco, J. A.; Lee, J.; Armstrong, C. M.; Gehring, A. G. *Anal. Bioanal. Chem.* **2019**, *411*, 5233−5242.
(6) Muniandy, S.; Teh, S. J.; Thong, K. L.; Thiha, A.; Dinshaw, I. J.; Lai, C. W.; Ibrahim, F.; Leo, B. F. *Crit. Rev. Anal. Chem.* **2019**, *49*, 510−533.
(7) Diaz-Amaya, S.; Zhao, M.; Lin, L. K.; Ostos, C.; Allebach, J. P.; Chiu, G. T. C.; Deering, A. J.; Stanciu, L. A. *Small* **2019**, *15*, No. 1805342.
(8) Xue, L.; Huang, F. C.; Hao, L.; Cai, G. Z.; Zheng, L. Y.; Li, Y. B.; Lin, J. H. *Food Chem.* **2020**, *322*, No. 126719.
(9) Chen, Y. P.; Xianyu, Y. L.; Dong, M. L.; Zhang, J. J.; Zheng, W. S.; Qian, Z. Y.; Jiang, X. Y. *Anal. Chem.* **2018**, *90*, 6906−6912.
(10) Perez, J. M.; Simeone, F. J.; Saeki, Y.; Josephson, L.; Weissleder, R. *J. Am. Chem. Soc.* **2003**, *125*, 10192−10193.
(11) Chen, Y. P.; Yin, B. F.; Dong, M. L.; Xianyu, Y. L.; Jiang, X. Y. *Anal. Chem.* **2018**, *90*, 1234−1240.
(12) Dong, M. L.; Zheng, W. S.; Chen, Y. P.; Ran, B.; Qian, Z. Y.; Jiang, X. Y. *Anal. Chem.* **2018**, *90*, 2833−2838.
(13) Wang, Z. L.; Xianyu, Y. L.; Zhang, Z.; Guo, A. L.; Li, X. J.; Dong, Y. Z.; Chen, Y. P. *ACS Sens.* **2019**, *4*, 2771−2777.
(14) Mahdavinia, G. R.; Mousanezhad, S.; Hosseinzadeh, H.; Darvishi, F.; Sabzi, M. *Carbohydr. Polym.* **2016**, *147*, 379−391.
(15) Fabra, M. J.; Perez-Bassart, Z.; Talens-Perales, D.; Martinez-Sanz, M.; Lopez-Rubio, A.; Marin-Navarro, J.; Polaina, J. *Food Hydrocolloids* **2019**, *96*, 171−177.
(16) Rassu, G.; Salis, A.; Porcu, E. P.; Giunchedi, P.; Roldo, M.; Gavini, E. *Carbohydr. Polym.* **2016**, *136*, 1338−1347.
(17) Hernandez-Gonzalez, A. C.; Tellez-Jurado, L.; Rodriguez-Lorenzo, L. M. *Carbohydr. Polym.* **2020**, *229*, No. 115514.
(18) Chang, Z. T.; Chen, Y. J.; Tang, S. X.; Yang, J. Y.; Chen, Y.; Chen, S. S.; Li, P. W.; Yang, Z. M. *Carbohydr. Polym.* **2020**, *229*, No. 115431.
(19) Qu, J.; Zhao, X.; Liang, Y. P.; Zhang, T. L.; Ma, P. X.; Guo, B. L. *Biomaterials* **2018**, *183*, 185−199.
(20) Mao, X. X.; Chen, G. F.; Wang, Z. H.; Zhang, Y. G.; Zhu, X. L.; Li, G. X. *Chem. Sci.* **2018**, *9*, 811−818.
(21) Langford, G. J.; Raeburn, J.; Ferrier, D. C.; Hands, P. J. W.; Shaver, M. P. *ACS Sens.* **2019**, *4*, 185−191.
(22) Gosset, A.; Oestreicher, V.; Perullini, M.; Bilmes, S. A.; Jobbagy, M.; Dulhoste, S.; Bayard, R.; Durrieu, C. *Anal. Methods* **2019**, *11*, 6193−6203.
(23) Tang, S. X.; Yang, J. Y.; Lin, L. Z.; Peng, K. L.; Chen, Y.; Jin, S. H.; Yao, W. S. *Chem. Eng. J.* **2020**, *393*, No. 124728.
(24) Marquez, A.; Jimenez-Jorquera, C.; Dominguez, C.; Munoz-Berbel, X. *Biosens. Bioelectron.* **2017**, *97*, 136−142.
(25) Xu, J.; Hu, X. T.; Khan, H.; Tian, M. M.; Yang, L. *Anal. Chim. Acta* **2019**, *1071*, 1−7.
(26) Wang, W. J.; Qian, J. C.; Tang, A. M.; An, L. N.; Zhong, K.; Liang, G. L. *Anal. Chem.* **2014**, *86*, 5955−5961.
(27) Si, Y.; Wang, L. H.; Wang, X. Q.; Tang, N.; Yu, J. Y.; Ding, B. *Adv. Mater.* **2017**, *29*, No. 1700339.
(28) Han, X. Q.; Huang, J. P.; To, A. K. W.; Lai, J. H. C.; Xiao, P.; Wu, E. X.; Xu, J. D.; Chan, K. W. Y. *Theranostics* **2020**, *10*, 2215−2228.
(29) Yang, J. Q.; Hu, X. T.; Xu, J.; Liu, X.; Yang, L. *Anal. Chem.* **2018**, *90*, 4071−4078.
(30) Zhang, Z. P.; Zhang, R. J.; Zou, L. Q.; McClements, D. J. *Food Hydrocolloids* **2016**, *58*, 308−315.
(31) Nie, R. B.; Xu, X. X.; Chen, Y. P.; Yang, L. *ACS Sens.* **2019**, *4*, 1864−1872.
(32) Zhang, L. H.; Chen, C. W.; Zhang, G. L.; Liu, B.; Wu, Z. Y.; Cai, D. Q. *J. Agric. Food Chem.* **2020**, *68*, 1536−1545.

https://doi.org/10.1021/acs.analchem.0c03968
Anal. Chem. 2021, 93, 6613−6619